Image contrast assessment of metal-based nanoparticles as applications for image-guided radiation therapy

Nakayama, Masao ; Akasaka, Hiroaki ; Miyazaki, Eiichi ; Goto, Yoshihiro ; Oki, Yuya ; Kawate, Yosuke ; Morita, Kenta ; Sasaki, Ryohei

(URL)
https://hdl.handle.net/20.500.14094/90008881
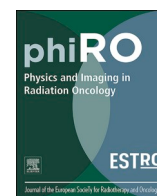
Technical Note

Image contrast assessment of metal-based nanoparticles as applications for image-guided radiation therapy

Masao Nakayama [a,b,*], Hiroaki Akasaka [b,c], Eiichi Miyazaki [a], Yoshihiro Goto [d], Yuya Oki [c], Yosuke Kawate [c], Kenta Morita [e], Ryohei Sasaki [b]

[a] *Division of Radiation Therapy, Kita-Harima Medical Center, 926-250 Ichibacho, Ono, Hyogo 675-1392, Japan*
[b] *Division of Radiation Oncology, Kobe University Graduate School of Medicine, 7-5-2 Kusunokicho, Chuou-ku, Kobe, Hyogo 650-0017, Japan*
[c] *Division of Radiation Oncology, Kobe Minimally Invasive Cancer Center, 8-5-1 Minatojima-Nakamachi, Chuou-ku, Kobe, Hyogo 650-0046, Japan*
[d] *Department of Radiology, Kita-Harima Medical Center, 926-250 Ichibacho, Ono, Hyogo 675-1392, Japan*
[e] *Department of Chemical Science and Engineering, Graduate School of Engineering, Kobe University, 1-1 Rokkodaicho, Nada-ku, Kobe, Hyogo 657-8501, Japan*

A B S T R A C T

Metal-based nanoparticles (NPs) have been extensively studied for dose enhancement applications in radiation therapy. This study investigated the utility of such NPs for image-guided radiation therapy (IGRT). Phantom images of gold NPs (AuNPs) and titanium peroxide NPs (TiOxNPs) with different concentrations were acquired using IGRT modalities, including cone-beam computed tomography (CBCT). AuNPs induced strong contrast enhancement in kV energy CBCT images, whereas TiOxNPs at high concentrations showed weak but detectable changes. The results indicated that these NPs can be used to enhance IGRT images as well as dose enhancement for treatment purposes.

1. Introduction

Nanoparticles (NPs) have been extensively studied for their use as radiosensitising agents in radiation therapy against cancer [1]. In the reaction with X-rays, metal NPs can generate secondary electrons and consequently reactive oxygen species (ROS) through radiolysis of water molecules, which can damage cancer cells and enhance the X-ray effects [2]. Along with the dose enhancement effects in radiation therapy, their radiosensitising properties can act as potential agents for enhancing the image contrast in computed tomography (CT) because of the X-ray absorption with metal atoms [3]. Thus, by combining these therapeutic and diagnostic enhancements, NPs have been explored for possible theranostic applications.

In current radiation therapy clinical practice, imaging techniques are increasingly used for patient set-up corrections as part of image-guided radiation therapy (IGRT) [4]. Cone-beam CT (CBCT) is among the most common IGRT techniques that allow precise patient set-up and minimisation of interfractional organ motions before the delivery of treatment beams. While standard diagnostic CT uses a fan beam with a helical beam path to scan the patient, CBCT images are acquired with a single rotation of the kV X-ray source and detector, mounted on linear

accelerator (linac) units. Moreover, megavoltage CT (MVCT) using high-energy beams from the linac are also available depending on treatment devices. As IGRT is performed during radiation therapy sessions, metal NPs, which are loaded to enhance the radiation dose in the tumour, can enhance the image contrast in IGRT modalities as well and assist the image registration process by visualising the clear tumour location in soft tissues.

The radiosensitising effects of gold NPs (AuNPs) have been demonstrated in many studies [5–7]. In addition to their therapeutic dose enhancement in radiation therapy, diagnostic enhancement in CT images has also been reported in several studies [8–10]. Although previous studies have used standard diagnostic CT or small animal CT scanners to assess the image contrast ability of AuNPs, none of them have investigated the contrast enhancement in IGRT imaging modalities using AuNPs and other NPs. The aim of this study was therefore to evaluate the contrast ability of metal NPs on IGRT modalities including CBCT and MVCT. Two different types of NPs were employed: AuNPs as high atomic number NPs and titanium peroxide nanoparticles (TiOxNPs) as low atomic number NPs. TiOxNPs were originally synthesised from titanium dioxide nanoparticles (TiO$_2$NPs) with hydrogen peroxide (H$_2$O$_2$) as novel agents for enhancing radiation effects [11]. Owing to their unique

---

ability to generate or release H_2O_2, they have shown promising dose enhancement under X-ray irradiation *in vitro* and *in vivo* studies [11–13]. Thus, in this study, TiOxNPs were considered a suitable specimen to investigate their image contrast properties as well as AuNPs.

2. Material and methods

2.1. Preparation of NPs

AuNPs were purchased from Nanoprobes (AuroVist™, lot number 06S700, Yaphank, NY, USA) and diluted to obtain a concentration of 40 mg/ml using phosphate-buffered saline. According to manufacturer's instructions, a water-soluble organic ligand shell is coordinated on the gold core. TiOxNPs were synthesised based on a method described in our previous research [11]. The surface of TiOxNPs was functionalised using polyacrylic acid, in accordance with our previous studies [14,15]. The sizes of AuNPs and TiOxNPs were approximately 15 and 50 nm, respectively (supplementary Fig. 1). Final concentrations of NPs used in this phantom study were 0, 1, 5, and 10 mg/ml for each NPs sample, diluted using purified water to achieve the required concentrations.

2.2. Imaging modalities

Four different types of medical imaging modalities were applied in this study: standard diagnostic CT, linac-integrated kilovoltage cone-beam CT (CBCT), megavoltage CT (MVCT) in helical tomotherapy, and standard diagnostic magnetic resonance imaging (MRI). Although MRI-linac is on the way to becoming one of the common IGRT modalities [16,17] it was not available in any of our centres, thus, a standard MRI system was used for this study instead. Two milliliters of NP solution for each concentration was placed in holes of a water-equivalent cylinder phantom with a diameter of 15 cm. Thereafter, the phantom was scanned using the imaging modalities. Diagnostic CT images were obtained using an Optima CT580 scanner (GE Healthcare, Waukesha, WI, USA) with a tube potential of 120 kVp and two different tube currents of 100 and 400 mA (for head and body scan protocols, respectively). CBCT images were acquired using two types of Varian linac: Clinac iX and TrueBeam (Varian Medical Systems, Palo Alto, CA, USA). Furthermore, half- and full-rotation CBCT scans were performed with standard acquisition protocols. MVCT images were obtained using Tomotherapy (Accuray, Sunnyvale, CA, USA), wherein 3.5 MV X-ray beams were available for the image guidance [18]. The obtained CT images were imported into the Eclipse software (version 15.6, Varian Medical Systems, Palo Alto, CA, USA) and the Hounsfield units (HUs) for each sample were measured using five different axial slices. The data were represented as mean ± standard deviation. In addition to CT images, T1- and T2-weighted images were acquired using a MAGNETOM Avanto 1.5T MRI scanner (Siemens AG, Munich, Germany) with a turbo spin-echo sequence. Scan parameters for each imaging modality were based on routine clinical settings. The details are summarised in Supplementary Table 1.

2.3. Contrast visibility test

The visibility of AuNPs and TiOxNPs on CT images was assessed to determine whether they were feasible as image contrast agents for clinical use. We prepared a CT image, wherein two samples of NPs and eight samples of water were randomly arranged. Subsequently, four certified medical physicists independently selected two out of the ten samples, thought to be NPs. This test was replicated for different concentrations of the NPs and different sets of CT window width and level (WW/WL). The visibility of the NPs was calculated as a percentage of correct answers. The contrast-to-noise ratio (CNR) was also calculated for quantitative measures [19].

3. Results

For both AuNPs and TiOxNPs the contrast levels in CBCT images were the same as those for standard diagnostic CT regardless of scan parameters (Fig. 1A). Large fluctuations observed on CT attenuation at 1 mg/ml for both NPs were due to nonuniformity and noise of CBCT images. The absolute values of the HUs increased linearly, depending on NP concentrations in both AuNPs and TiOxNPs (supplementary Fig. 2A-F). The overall mean slopes were 26.4 ± 1.3 and 2.7 ± 0.7 HU/(mg/ml) for AuNPs and TiOxNPs, respectively. Evidently, the enhancement effect of AuNPs was much higher than that of TiOxNPs. The HUs of these NPs on MVCT images were much lower than those on the kV CT images, and no visible differences were observed. While the HUs increased linearly with NP concentration on MVCT images (supplementary Fig. 2G), the slopes of linear fits were 1.0 and 0.3 HU/(mg/ml) for AuNPs and TiOxNPs, respectively. Typical NPs images of CT, CBCT, and MVCT are represented in Fig. 1B. Moreover, in T2-weighted MR image, TiOxNPs were negatively enhanced, whereas there were no differences in AuNPs (Fig. 1B and 1C).

The visibility test result showed that images of AuNPs were correctly identified from control images at all concentrations. The contrast of TiOxNPs could be almost visible at the concentrations of 5 and 10 mg/ml on images with a liver window setting; however, that of 1 mg/ml had a poor correct rate with a very low CNR, indicating no visible contrast at this concentration. The visibility and CNR for both NPs are summarised in Table 1.

4. Discussion

This study showed the potential ability of two different types of metal NPs as contrast agents in IGRT modalities. As expected, AuNPs had visible contrast in CBCT images regardless of exposure settings as well as in diagnostic CT images. The results were similar to a previous
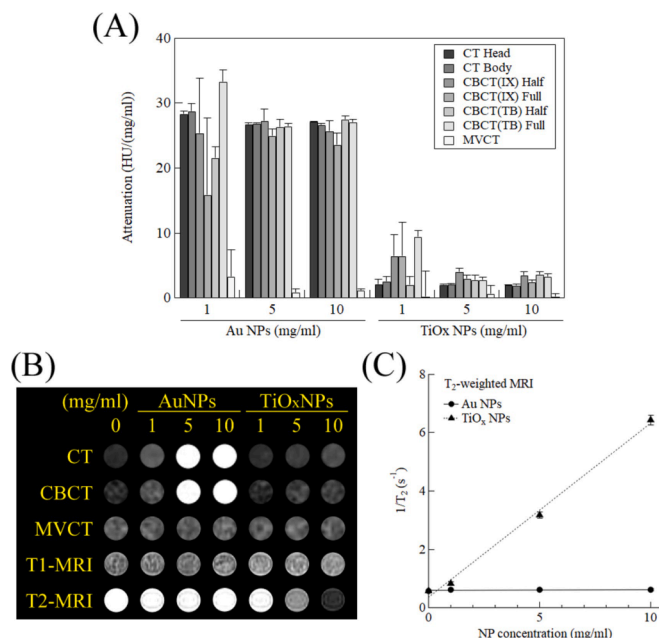

Fig. 1. Contrast enhancements induced by AuNPs and TiOxNPs. (A) CT attenuation for AuNPs and TiOxNPs on different modalities and scan settings. IX, Clinac iX; TB, TrueBeam. (B) Representative images in standard CT (head scan), CBCT (TrueBeam, half scan), MVCT, T1-weighted MRI, and T2-weighted MRI. The standard CT and CBCT images are displayed with a liver window setting (WW/WL = 150/50), and the MVCT images are displayed with an abdomen window setting (WW/WL = 350/50). (C) T2 relaxation rates as a function of the concentration of NPs. Data are represented as mean ± standard deviation obtained from five different axial slices.

Table 1
Visibility of AuNPs and TiOxNPs in a CT phantom image.

NPs	Concentration	CNR	WW/WL	Visibility (%)
AuNPs	1 mg/ml	7.4	Abdomen	100
			Liver	100
			Pelvis	75
	5 mg/ml	35.8	Abdomen	100
			Liver	100
			Pelvis	100
	10 mg/ml	72.9	Abdomen	100
			Liver	100
			Pelvis	100
TiOxNPs	1 mg/ml	0.6	Abdomen	12.5
			Liver	0
			Pelvis	0
	5 mg/ml	2.9	Abdomen	12.5
			Liver	75
			Pelvis	25
	10 mg/ml	5.9	Abdomen	50
			Liver	100
			Pelvis	50

CNR, contrast-to-noise ratio; WW, window width; WL, window level. WW/WL = 350/50, 150/50, 400/40 for abdomen, liver, and pelvis settings, respectively.

study by Dong et al., wherein enhanced image contrast was observed with the attenuation rate of 23.7 HU/(mg/ml) in diagnostic CT using 50 nm AuNPs [8]. They also demonstrated that different sizes of AuNPs caused no significant changes in X-ray attenuation using three different clinical CT systems with different tube potentials, possibly suggesting no size effects on the contrast enhancement in CBCT images, even though single-sized AuNPs were employed in our study. Despite the enhanced contrast of AuNPs in kV CT images, a low contrast enhancement could be observed in MVCT images even at a 10 mg/ml concentration of AuNPs. Theoretically, the Compton scattering becomes a dominant process for MV X-rays in the interaction with materials having a high atomic number, such as gold, and the X-ray cross-section is smaller than that in the interaction with kV energy photons, in which the photoelectric effect is dominant. In contrast to low X-ray attenuation of AuNPs in MVCT images, there are several *in vitro* studies that report significant radio-sensitising effects of AuNPs in response to MV X-ray irradiation [20,21]. The discrepancy between therapy and image contrast enhancements is possibly due to biological factors, including intracellular ROS and oxidative stress induced by AuNPs [22].

The contrast enhancement caused by TiOxNPs in CT images were much weaker than those by AuNPs. This was because titanium has lower atomic number ($Z = 22$) and mass attenuation coefficient ($\mu/\rho = 0.2721$ cm^2/g) than those of gold (79, 5.158 cm^2/g, respectively, at 100 keV photons) [23], resulting in less interaction with X-rays than gold. However, our qualitative results of the visibility test indicated that TiOxNPs with a concentration greater than 5 mg/ml could still be identified in certain soft tissues similar to water HU. The CNR of 3 is possibly a threshold for NPs contrast to be observable, which agrees with the Rose criterion [24]. A few studies have investigated the CT image contrast enhancement of TiO$_2$NPs which are foundational materials of TiOxNPs. One previous study evaluated it with up to 1 mg/ml TiO$_2$NPs and found no visible changes in standard CT images [25], whereas another study showed that TiO$_2$NPs with a concentration of 15 mg/ml had 26.6 $\pm$ 4 HU in CT images indicating that they were detectable on a CT scanner even at low concentrations [26]. Our results for TiOxNPs were similar to those of previous studies as TiOxNPs caused visible changes in CT images at high concentrations. However, TiOxNPs induced negative contrast in T2-weighted MRI, whereas AuNPs did not. Our previous study using TiO$_2$NPs also demonstrated the change in T2 relaxation time with TiO$_2$NPs [25]. The negative enhancement of NPs may show darkened tumour regions in T2-weighted MRI, when they are used as radiosensitisers for tumours, which may be, however, unfavourable in IGRT using MRI-linac.

There are several limitations in this study. The contrast

enhancements were assessed in a phantom with uniform contrast around NPs samples; however, visual appearances may be changed in a human body where surrounding tissues have different contrast. Similar to other *in vivo* studies that demonstrated the contrast enhancement of AuNPs in CT images using mice [3,27], future studies should be conducted to determine the contrast enhancement ability of NPs with subsequent image registration in clinical situations using IGRT modalities. Another limitation is cellular cytotoxicity of NPs at high concentrations, which is not considered in this study as phantom-based experiments. While a higher concentration of NPs may cause higher contrast enhancement in images, it can also increase cytotoxicity in cells. Therefore, *in vitro* and *in vivo* studies are warranted to find optimal concentrations of NPs as a clinical theranostic agent in future.

In conclusion, both AuNPs and TiOxNPs had contrast enhancement in kV energy CBCT images as well as in standard diagnostic CT images, whereas there was a dependence on the NP concentration. Furthermore, the findings indicate that metal NPs can be possibly utilised during image registration process in IGRT practice, and can sequentially enhance the irradiated dose for treatment.

Conflicts of interest

None.

Declaration of Competing Interest

The authors declare that they have no known competing financial interests or personal relationships that could have appeared to influence the work reported in this paper.

Appendix A. Supplementary data

Supplementary data to this article can be found online at https://doi.org/10.1016/j.phro.2021.11.003.

References

[1] Liu Y, Zhang P, Li F, Jin X, Li J, Chen W, et al. Metal-based nanoenhancers for future radiotherapy: radiosensitizing and synergistic effects on tumor cells. Theranostics 2018;8:1824–49. https://doi.org/10.7150/thno.22172.

[2] Howard D, Sebastian S, Le QV-C, Thierry B, Kempson I. Chemical mechanisms of nanoparticle radiosensitization and radioprotection: a review of structure-function relationships influencing reactive oxygen species. Int J Mol Sci 2020;21:579. https://doi.org/10.3390/ijms21020579.

[3] Dou Y, Guo Y, Li X, Li X, Wang S, Wang L, et al. Size-tuning ionization to optimize gold nanoparticles for simultaneous enhanced CT imaging and radiotherapy. ACS Nano 2016;10:2536–48. https://doi.org/10.1021/acsnano.5b07473.

[4] Potters L, Gaspar LE, Kavanagh B, Galvin JM, Hartford AC, Hevezi JM, et al. American society for therapeutic radiology and oncology (ASTRO) and American college of radiology (ACR) practice guidelines for image-guided radiation therapy (IGRT). Int J Radiat Oncol Biol Phys 2010;76:319–25. https://doi.org/10.1016/j.ijrobp.2009.09.041.

[5] Hainfeld JF, Slatkin DN, Smilowitz HM. The use of gold nanoparticles to enhance radiotherapy in mice. Phys Med Biol 2004;49:N309–15. https://doi.org/10.1088/0031-9155/49/18/N03.

[6] Cui L, Her S, Borst GR, Bristow RG, Jaffray DA, Allen C. Radiosensitization by gold nanoparticles: Will they ever make it to the clinic? Radiother Oncol 2017;124:344–56. https://doi.org/10.1016/j.radonc.2017.07.007.

[7] Chen Y, Yang J, Fu S, Wu J. Gold Nanoparticles as Radiosensitizers in cancer radiotherapy. Int J Nanomed 2020;15:9407–30. https://doi.org/10.2147/IJN.S272902.

[8] Dong YC, Hajfathalian M, Maidment PSN, Hsu JC, Naha PC, Si-Mohamed S, et al. Effect of gold nanoparticle size on their properties as contrast agents for computed tomography. Sci Rep 2019;9. https://doi.org/10.1038/s41598-019-50332-8.

[9] Oumano M, Russell L, Salehjahromi M, Shanshan L, Sinha N, Ngwa W, et al. CT imaging of gold nanoparticles in a human-sized phantom. J Appl Clin Med Phys 2021;22:337–42. https://doi.org/10.1002/acm2.13155.

[10] Khademi S, Sarkar S, Kharrazi S, Amini SM, Shakeri-Zadeh A, Ay MR, et al. Evaluation of size, morphology, concentration, and surface effect of gold nanoparticles on X-ray attenuation in computed tomography. Phys Med 2018;45: 127–33. https://doi.org/10.1016/j.ejmp.2017.12.001.

[11] Nakayama M, Sasaki R, Ogino C, Tanaka T, Morita K, Umetsu M, et al. Titanium peroxide nanoparticles enhanced cytotoxic effects of X-ray irradiation against pancreatic cancer model through reactive oxygen species generation in vitro and in vivo. Radiat Oncol 2016;11. https://doi.org/10.1186/s13014-016-0666-y.

[12] Hassan M, Nakayama M, Salah M, Akasaka H, Kubota H, Nakahana M, et al. A comparative assessment of mechanisms and effectiveness of radiosensitization by titanium peroxide and gold nanoparticles. Nanomaterials 2020;10:1125. https://doi.org/10.3390/nano10061125.

[13] Morita K, Nishimura Y, Nakamura S, Arai Y, Numako C, Sato K, et al. Titanium oxide nano-radiosensitizers for hydrogen peroxide delivery into cancer cells. Colloids Surf B Biointerfaces 2021;198:111451. https://doi.org/10.1016/j.colsurfb.2020.111451.

[14] Morita K, Suzuki T, Nishimura Y, Matsumoto K, Numako C, Sato K, et al. In vivo tissue distribution and safety of polyacrylic acid-modified titanium peroxide nanoparticles as novel radiosensitizers. J Biosci Bioeng 2018;126:119–25. https://doi.org/10.1016/j.jbiosc.2018.01.012.

[15] Morita K, Miyazaki S, Numako C, Ikeno S, Sasaki R, Nishimura Y, et al. Characterization of titanium dioxide nanoparticles modified with polyacrylic acid and H_2O_2 for use as a novel radiosensitizer. Free Radical Res 2016;50:1319–28. https://doi.org/10.1080/10715762.2016.1241879.

[16] Raaymakers BW, Lagendijk JJW, Overweg J, Kok JGM, Raaijmakers AJE, Kerkhof EM, et al. Integrating a 1.5 T MRI scanner with a 6 MV accelerator: proof of concept. Phys Med Biol 2009;54:N229–37. https://doi.org/10.1088/0031-9155/54/12/N01.

[17] van Herk M, McWilliam A, Dubec M, Faivre-Finn C, Choudhury A. Magnetic resonance imaging-guided radiation therapy: a short strengths, weaknesses, opportunities, and threats analysis. Int J Radiat Oncol Biol Phys 2018;101: 1057–60. https://doi.org/10.1016/j.ijrobp.2017.11.009.

[18] Langen KM, Papanikolaou N, Balog J, Crilly R, Followill D, Goddu SM, et al. QA for helical tomotherapy: report of the AAPM Task Group 148. Med Phys 2010;37: 4817–53. https://doi.org/10.1118/1.3462971.

[19] Harun AZ, Rashid RA, Razak KA, Geso M, Rahman WN. Evaluation of contrast-noise ratio (CNR) in contrast enhanced CT images using different sizes of gold nanoparticles. Mater Today: Proc 2019;16:1757–65. https://doi.org/10.1016/j.matpr.2019.06.046.

[20] Jain S, Coulter JA, Hounsell AR, Butterworth KT, McMahon SJ, Hyland WB, et al. Cell-specific radiosensitization by gold nanoparticles at megavoltage radiation energies. Int J Radiat Oncol Biol Phys 2011;79:531–9.

[21] Kazmi F, Vallis KA, Vellayappan BA, Bandla A, Yukun D, Carlisle R. Megavoltage radiosensitization of gold nanoparticles on a glioblastoma cancer cell line using a clinical platform. Int J Mol Sci 2020;21:429. https://doi.org/10.3390/ijms21020429.

[22] Butterworth KT, McMahon SJ, Taggart LE, Prise KM. Radiosensitization by gold nanoparticles: effective at megavoltage energies and potential role of oxidative stress. Transl Cancer Res 2013;2:269–79. https://doi.org/10.3978/j.issn.2218-676X.2013.08.03.

[23] Hubbell JH and Seltzer SM. Tables of X-ray mass attenuation coefficients (version 1.4). Online available: http://physics.nist.gov/xaamdi (2021/10/28). National Institute of Standards and Technology, Gaithersburg, MD.

[24] Cherry SR, Sorenson JA, Phelps ME. Image quality in nuclear medicine. In: Physics in nuclear medicine. 4th edition. Elsevier; 2012. https://doi.org/10.1016/B978-1-4160-5198-5.00015-0.

[25] Akasaka H, Mukumoto N, Nakayama M, Wang T, Yada R, Shimizu Y, et al. Investigation of the potential of using TiO_2 nanoparticles as a contrast agent in computed tomography and magnetic resonance imaging. Appl Nanosci 2020;10: 3143–8. https://doi.org/10.1007/s13204-019-01098-y.

[26] Leon S, Zdenka K, Kostya O, Shailesh K. Nanoparticles in cancer imaging and therapy. J Nanomater 2012:891318. https://doi.org/10.1155/2012/891318.

[27] Nakagawa T, Gonda K, Kamei T, Cong L, Hamada Y, Kitamura N, et al. X-ray computed tomography imaging of a tumor with high sensitivity using gold nanoparticles conjugated to a cancer-specific antibody via polyethylene glycol chains on their surface. Sci Technol Adv Mater 2016;17:387–97. https://doi.org/10.1080/14686996.2016.1194167.